2020 IEEE/RSJ International Conference on Intelligent Robots and Systems (IROS)
October 25-29, 2020, Las Vegas, NV, USA (Virtual)

2020 IEEE/RSJ International Conference on Intelligent Robots and Systems (IROS) | 978-1-7281-6212-6/20/$31.00 ©2020 IEEE | DOI: 10.1109/IROS45743.2020.9341476

Optimizing coordinate choice for locomotion systems with toroidal shape spaces

Bo Lin[1,*], Baxi Chong[2,*], Yasemin Ozkan-Aydin[2], Enes Aydin[2],
Howie Choset[3], Daniel I. Goldman[4], Greg Blekherman[1]

Abstract— In a geometric mechanics framework, the configuration space is decomposed into a shape space and a position space. The internal motion of the system is prescribed by a closed loop in the shape space, which causes net motion in the position space. If the shape space is a simply connected domain in an Euclidean space, then with an optimal choice of the body frame, the displacement in the position space is reasonably approximated by the surface integral of the height function, a functional relationship between the internal shape and position space variables. Our recent work has extended the scope of geometric methods from limbless undulatory system to those with legs; interestingly, the shape space for such systems has a torus structure. However, to the best of our knowledge, the optimal choice of the body frame on the torus shape space was not explored. In this paper, we develop a method to optimally choose the body frame on the torus which results in good approximation of displacement by the integral of the height function. We apply our methods to the centipede locomotion system and observe quantitative agreement of our prediction and experimental results.

I. Introduction

Recently, the geometric mechanics framework [2], [3], [4] has been successfully applied to study various locomotion behaviors, including limbless locomotion [3], and legged locomotion [5]. In this framework, the motion of a self-propelling system is separated into a shape space (the internal joint-angle space) and a position space (position and orientation of a locomotor in the world frame). A gait then maps closed loop path in the shape space to displacement in the position space. To visually analyze the gait, Shammas et. al [6] numerically calculated the height function over the shape space and approximate displacement by the integral of the height function over the area enclosed by the gait path.

The integral of the height function provides an approximation, but is not exact, because the system's position space is $SE(2)$ whose group structure is not commutative. In other words, translation and rotation motion, in the plane, are separately commutative (i.e. motion in x and then y, is the same as motion in y and then x, or rotation in θ_1 followed by rotation in θ_2 is the same as rotation in θ_2 followed by rotation in θ_1), but when combined, translation and rotation motion do not commute. More technically, the choice of an optimal frame mitigates the non-commutative effects of motion making the integral of the height function is good. Instead, the displacement in the position space should be described as the sum of the height function integral, the Lie bracket term [2] and higher order terms. It was shown in [2], [4] that when the shape space is a simply connected domain in the Euclidean space, the Lie bracket term and higher order term can be minimized by optimally choosing a body frame.

Recent work extended geometric mechanics framework to torus shape spaces [7], which allowed for study of a broader range of locomotors. For example, Ozkan-Aydin et. al, [1] applied the work of Gong et. al. [7] to study

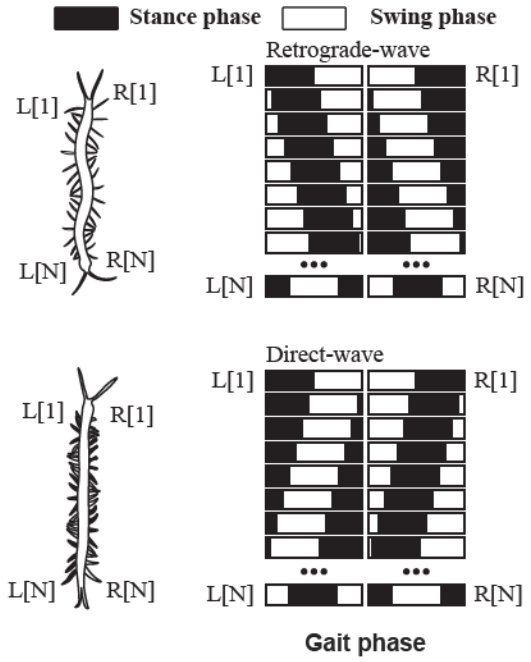

Fig. 1. Gait diagram of the retrograde-wave of scolopendra polymorpha (top) and direct-wave of Scolopocryptops sexspinosous (bottom). Filled blocks represent stance phase, open blocks represent swing phase.

*These authors contributed equally to this work.

[1] Bo Lin and Greg Blekherman are with Faculty of School of Mathematics, Georgia Institute of Technology, and Southeast Center for Mathematics and Biology (SCMB), Atlanta, GA 30332, USA {bo.lin, greg}@math.gatech.edu

[2] Baxi Chong, Yasemin Ozkan-Aydin and Enes Aydin are with the School of Physics, Georgia Institute of Technology, Atlanta, GA 30332, USA {bchong9, yaydin6, eaydin7}@gatech.edu

[3] Howie Choset is with Faculty of the Robotics Institute, Carnegie Mellon University, Pittsburgh, PA 15213, USA choset@ri.cmu.edu

[4] Daniel I. Goldman is with Faculty of the School of Physics, Georgia Institute of Technology, and Southeast Center for Mathematics and Biology (SCMB), Atlanta, GA 30332, USA daniel.goldman@physics.gatech.edu

Authorized licensed use limited to: Georgia Institute of Technology. Downloaded on June 17,2021 at 16:03:22 UTC from IEEE Xplore. Restrictions apply.

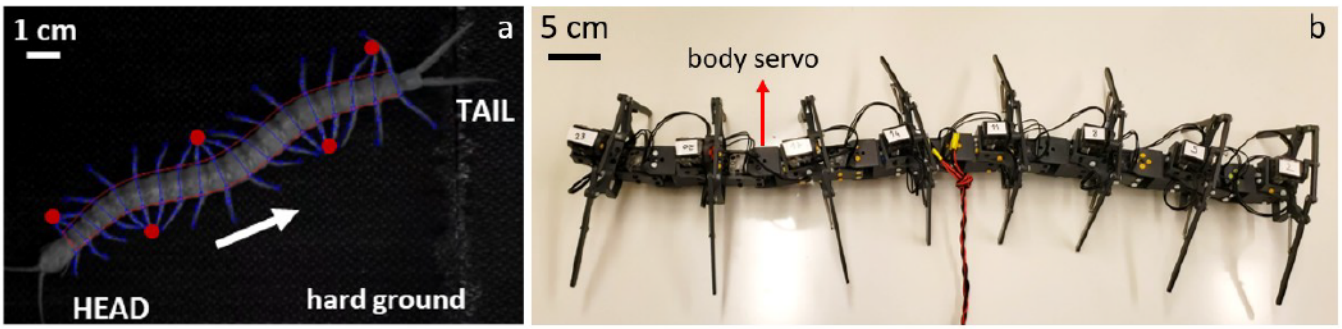

Fig. 2. Animal and robot centipede on flat terrain. (a) The North American centipede (Scolopendra polymorpha) is locomoting on a flat terrain with a retrograde body wave (propagating in the opposite direction of movement).Red dots show the points of contact with the ground. (by the courtesy of P. Schiebel, M. Brown and J. R. Mendelson III) (b) Robophysical model of a centipede. The robot has eight segments with a pair of legs in each (see [1] for the details). The lateral undulation of the body is controlled by body servos.

centipede locomotion and design gaits to coordinate the lateral body undulation and the leg movements. However, the work in [7] did not consider reducing the Lie bracket effect for the torus shape space, which may lead to inaccurate prediction of the displacement by the surface integral of the height function. For instance, the surface integral of the height function in [1] did not agree quantitatively with the experimental data.

In this paper we introduce a numerical method for finding the optimal body frame on the torus to minimize the Lie bracket effect. We demonstrate the usefulness of this procedure with refined analysis of centipede locomotion. A careful study of centipedes suggested that the centipede locomotion can be classified into two groups (see Fig. 1) [8], [9], [10]: the direct-wave (the leg wave propagates from tail to head) and the retrograde-wave (the leg wave propagates from head to tail).

Experiments in [1] (see Fig. 2 and 3) showed that retrograde-wave locomotion results in higher forward speed. However, the surface integral over the height functions in [1] does not distinguish between the speeds in direct-wave and retrograde-wave locomotion. We show numerically that an optimal choice of the body frame not only predicts higher forward speed for retrograde-wave centipedes, but also leads to the quantitative agreement between the surface integral and the experimental data.

This paper is organized as follows: in Section II we describe the optimization problem mathematically, then in Section III we describe the procedure of approximating the optimal body frame using the finite-element method. In Section IV we apply our optimization procedure to study the centipede locomotion and show that our predictions have quantitative agreement with experimental robot results of [1]. Finally in Section V, we consider the efficiency and generalizations of our method.

II. The Problem

A. Background

In this section, we provide a concise overview of the geometric tools needed for this paper. For a more detailed and comprehensive review, we refer readers to [7], [2], [4].

In kinematic systems where the inertia is negligible in the system, the equations of motion [11] reduce to

$$\boldsymbol{\xi} = \boldsymbol{A}(\boldsymbol{r})\dot{\boldsymbol{r}}, \tag{1}$$

where $\boldsymbol{\xi} = [\xi_x \ \xi_y \ \xi_\theta]^T$ denotes the body velocity in forward, lateral, and rotational directions in the designated body frame; $\boldsymbol{r}$ denotes the internal shape variable; $\boldsymbol{A}(\boldsymbol{r})$ is the local form of the connection matrix that relates shape velocity $\dot{\boldsymbol{r}}$ to body velocity $\boldsymbol{\xi}$. Often, for simplicity of visualization, we assume that the shape variable is two dimensional, i.e., $\boldsymbol{r} = (r_1, r_2)^T$. Note that the local form of the connection, $\boldsymbol{A}(\boldsymbol{r})$, depends on the choice of the body frame. (1) is also called the kinematic reconstruction equation and maps the changes in internal shape variables (joint angles) to changes in group variables (position and orientation) of the robot. Prior work [3] has shown that numerically derived local form of the connections using granular resistive force theory (RFT) can effectively predict movements in granular media. In this paper, we model the robot-ground contact by anisotropic Coulomb friction [12], [13], from which we numerically derive the local form of the connections.

Each row of the local form of the connection matrix $\boldsymbol{A}$ corresponds to a component direction [3] of the body velocity and therefore gives rise to a connection vector field. The body velocities in the forward, lateral and rotational directions are respectively computed as the dot product of connection vector fields and the shape velocity $\dot{\boldsymbol{r}}$. A shape velocity $\dot{\boldsymbol{r}}$ along the direction of the vector field yields the largest possible body velocity, while a shape velocity $\dot{\boldsymbol{r}}$ orthogonal to the field produces zero body velocity.

A gait can be represented as a closed curve in the corresponding shape space. The displacement resulting from a gait, $\partial\chi$, can be approximated by the body velocity integral:

$$\begin{pmatrix}\Delta x\\ \Delta y\\ \Delta\theta\end{pmatrix} \approx \int_{\partial\chi} \boldsymbol{A}(\boldsymbol{r})d\boldsymbol{r}. \tag{2}$$

Authorized licensed use limited to: Georgia Institute of Technology. Downloaded on June 17,2021 at 16:03:22 UTC from IEEE Xplore. Restrictions apply.

According to Stokes' Theorem, the line integral along a closed curve $\partial\chi$ is equal to the surface integral of the curl of $\boldsymbol{A}(\boldsymbol{r})$ over the surface enclosed by $\partial\chi$:

$$\int_{\partial\chi} \boldsymbol{A}(\boldsymbol{r})d\boldsymbol{r} = \iint_{\chi} \boldsymbol{\nabla}\times\boldsymbol{A}(\boldsymbol{r})dr_1dr_2, \tag{3}$$

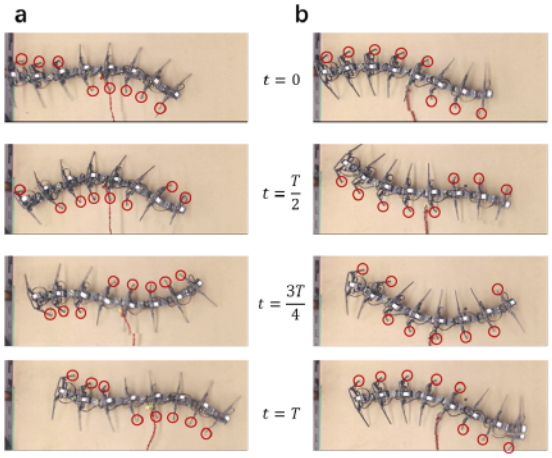

Fig. 3. Robot experiments on flat hard ground. Snapshots from the experiments (a) Lateral phase lag (LFL) 0.9 (retrograde) and (b) LFL 0.1 (prograde) with duty factor 50% of a period T on a flat particle board. Red dots show the legs on the ground. Red arrows show the directions of the waves.

where χ denotes the area enclosed by $\partial\chi$.

B. The optimization problem

The third row of the local form of the connection matrix $\boldsymbol{A}(\boldsymbol{r})$, $\boldsymbol{A_\theta}(\boldsymbol{r})$, represents the vector field that gives the rotation. As discussed in [4], the Lie bracket effect is neglected in the approximation in (1). Hatton et. al. showed that the Lie bracket effect can be minimized when the designated body frame is properly chosen [2]. The transformation of body frame orientation can be interpreted as, replacing the vector filed $\boldsymbol{A_\theta}(\boldsymbol{r})$ by a new vector field, $\boldsymbol{A'_\theta}(\boldsymbol{r})$ such that the line integral of $\boldsymbol{A'_\theta}(\boldsymbol{r})$ should be equal to the one of $\boldsymbol{A_\theta}(\boldsymbol{r})$ along any closed curve in the shape space. By the linearity of line integrals, $\boldsymbol{A_\theta}(\boldsymbol{r}) - \boldsymbol{A'_\theta}(\boldsymbol{r})$ is a vector field whose line integral along any closed curve is zero. By [14, Thm 2.1, p.362], $\boldsymbol{A_\theta}(\boldsymbol{r}) - \boldsymbol{A'_\theta}(\boldsymbol{r})$ is the gradient of some potential function, $P(\boldsymbol{r}) = P(r_1, r_2)$, defined on the shape space.

It is shown in [2] that in the optimal orientation of the body frame, the norm of the vector field $\boldsymbol{A'_\theta}$ is minimized. Let the vector field $\boldsymbol{A_\theta}(r_1, r_2) = (f_1(r_1, r_2), f_2(r_1, r_2))$ be the third row of $\boldsymbol{A}(\boldsymbol{r})$. Since the shape space of r_1, r_2 is the standard 2-torus T^2, which we identify with $(\mathbb{R}/2\pi\mathbb{Z}) \times (\mathbb{R}/2\pi\mathbb{Z}) = [0, 2\pi) \times [0, 2\pi)$. Now we need to minimize the 'distance' between F and the gradient $\nabla P(r_1, r_2)$ of a potential function $P(r_1, r_2)$ defined on T^2. For the efficiency of computations, we choose the L^2-norm, and thus our problem becomes:

Problem 1. Given continuous functions f_1, f_2 defined on T^2, find a differentiable function $P(r_1, r_2)$ defined on T^2 such that the integral

$$\int_{T^2} \left[\left(f_1(r_1,r_2) - \frac{\partial P}{\partial r_1}(r_1,r_2)\right)^2 + \left(f_2(r_1,r_2) - \frac{\partial P}{\partial r_2}(r_1,r_2)\right)^2\right] dr_1 dr_2 \tag{4}$$

is minimal.

III. The Method

Problem 1 is similar to the Helmholtz-Hodge decomposition [4, (B5)]. Nonetheless, the torus cannot be embedded into $\mathbb{R}^2$, and it is a manifold without boundary, so the standard Helmholtz-Hodge decomposition does nor apply. As a result, we cannot directly apply the decomposition, and our approach to Problem 1 would be an analogue of the Helmholtz-Hodge decomposition on the torus.

In practice, we cannot hope to have analytic formulas for f_1, f_2. So we need to look for numerical solutions. Since we only know the values of f_1, f_2 at finitely many points in T^2. As a result, we have to discretize the problem and solve for a discrete approximation of $P(r_1, r_2)$.

For suitable $n \in \mathbb{N}$, we can decompose $[0, 2\pi) \times [0, 2\pi)$ into a mesh of n^2 squares, and we focus on the lattices points $\left(\frac{2\pi i}{n}, \frac{2\pi j}{n}\right), 0 \le i, j \le n-1$. For sufficiently large n, the mesh is dense enough, and we try to find the values of a solution $P(r_1, r_2)$ at all those lattice points. For convenience, we denote the side length of squares in the mesh by $u = \frac{2\pi}{n}$.

Now we apply the finite-element method as in [2]. We define a family of basis functions $\phi_{i,j}$ such that $\phi_{i,j}$ takes value 1 at $\left(\frac{2\pi i}{n}, \frac{2\pi j}{n}\right)$ and 0 at all other lattice points.

The motivation of introducing $\phi_{i,j}$'s is Lemma 2.

Lemma 2. Suppose $P(r_1, r_2)$ takes value $c_{i,j}$ at $\left(\frac{2\pi i}{n}, \frac{2\pi j}{n}\right)$. Then at all lattice points

$$P(r_1, r_2) = \sum_{0\le i,j\le n-1} c_{i,j} \cdot \phi_{i,j}(r_1, r_2). \tag{5}$$

Our choice of the basis functions is the following: given integers $0 \le i, j \le n-1$, for all r_1, r_2 such that $\frac{2\pi(i-1)}{n} \le r_1 < \frac{2\pi(i+n-1)}{n}$, $\frac{2\pi(j-1)}{n} \le r_2 < \frac{2\pi(j+n-1)}{n}$, we define

$$\phi_{i,j}(r_1, r_2) = \max\left(1 - \frac{\left|r_1 - \frac{2\pi i}{n}\right|}{u}, 0\right) \cdot \max\left(1 - \frac{\left|r_2 - \frac{2\pi j}{n}\right|}{u}, 0\right). \tag{6}$$

Then $\phi_{i,j}$ is well-defined on T^2, only takes value 1 at the lattice point $\left(\frac{2\pi i}{n}, \frac{2\pi j}{n}\right)$ and takes value 0 at all other lattice points. In addition, $\phi_{i,j}$ is bilinear within each of the 4 quadrants around $\left(\frac{2\pi i}{n}, \frac{2\pi j}{n}\right)$.

Proof of Lemma 2. For any lattice point $\left(\frac{2\pi i_0}{n}, \frac{2\pi j_0}{n}\right)$, we have $\phi_{i,j}\left(\frac{2\pi i_0}{n}, \frac{2\pi j_0}{n}\right) = 1$ if $i = i_0$ and $j = j_0$, and $\phi_{i,j} = 0$ for all other choices of $0 \le i, j \le n-1$. So the right hand side of (5) equals $c_{i_0,j_0} \cdot 1 = c_{i_0,j_0} = P\left(\frac{2\pi i_0}{n}, \frac{2\pi j_0}{n}\right)$. □

Authorized licensed use limited to: Georgia Institute of Technology. Downloaded on June 17,2021 at 16:03:22 UTC from IEEE Xplore. Restrictions apply.

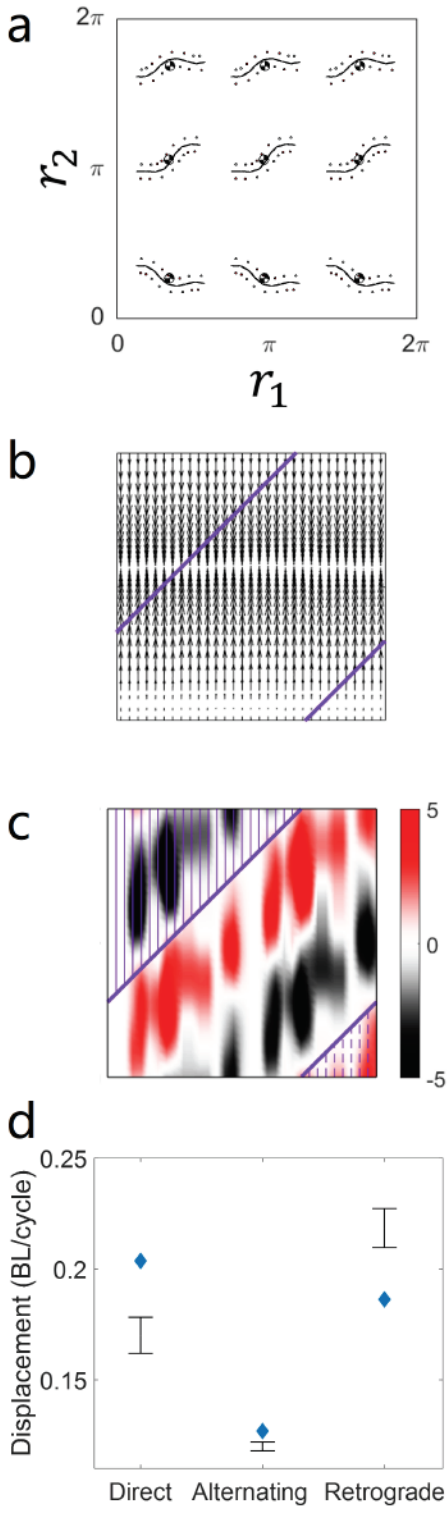

Fig. 4. Comparison of geometric mechanics prediction and the experimental data in the original frame. (a) The configuration of the robot in the body body frame (in this case, the head frame) on the shape space. (b) The vector field of the third row of the local form the the connection. (c) The forward height function in the original frame. The blue curve corresponds to the optimal $\partial\chi$ that enclosed the least surface in the upper left corner (shadowed in solid line) and the most surface in the lower right corner (shadowed in dashed line). Note that the labels and the axis in (b) an (c) is the same as in (a). (d) Comparison of the surface integral in the height function and the experimental data for direct-wave, alternating tripod and the retrograde-wave gaits.

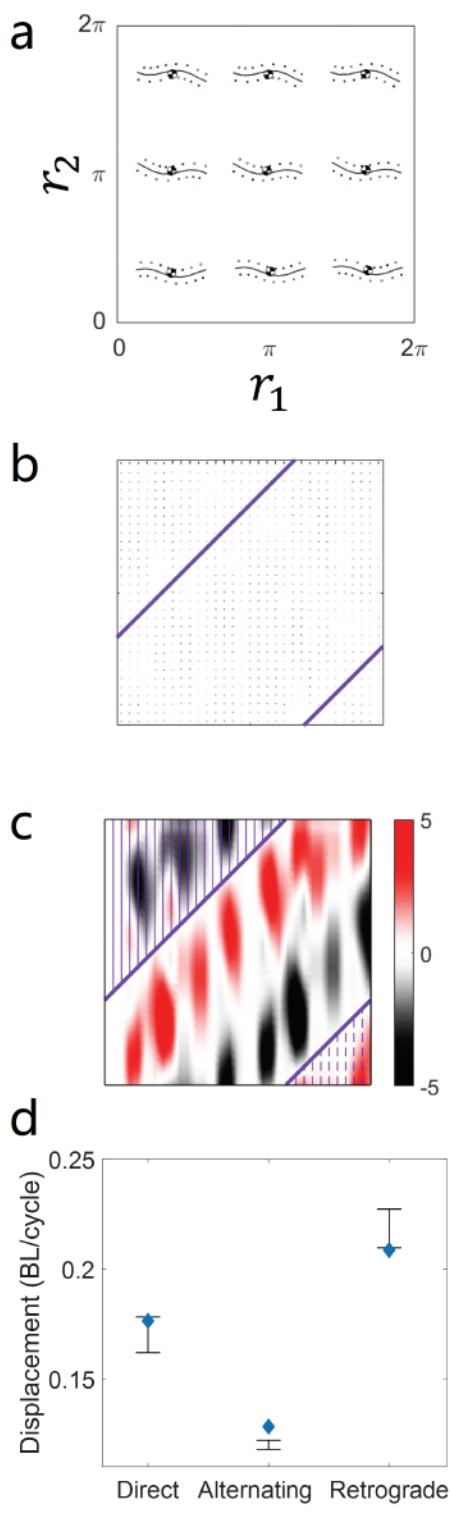

Fig. 5. Comparison of geometric mechanics prediction and the experimental data in the optimal frame. (a) The configuration of the robot in the optimal body frame on the shape space. (b) The vector field of the third row of the local form the the connection. (c) The forward height function in the optimal frame. The blue curve corresponds to the optimal $\partial\chi$ that enclosed the least surface in the upper left corner (shadowed in solid line) and the most surface in the lower right corner (shadowed in dashed line). Note that the labels and the axis in (b) an (c) is the same as in (a). (d) Comparison of the surface integral in the height function and the experimental data for direct-wave, alternating tripod and the retrograde-wave gaits.

Authorized licensed use limited to: Georgia Institute of Technology. Downloaded on June 17,2021 at 16:03:22 UTC from IEEE Xplore. Restrictions apply.

For convenience, for any two vector fields G, H defined on T^2, let their inner product be

$$\langle G,H\rangle=\int_{T^2}[G_1(r_1,r_2)H_1(r_1,r_2)+G_2(r_1,r_2)H_2(r_1,r_2)]\mathrm{d}r_1\mathrm{d}r_2.$$

Then $D = \langle \boldsymbol{A_\theta} - \nabla P, \boldsymbol{A_\theta} - \nabla P\rangle$. Now suppose a solution $P(r_1, r_2)$ is expressed as in (5). By the linearity of ∇ operator,

$$\nabla P = \sum_{0\le i,j\le n-1} c_{i,j}\cdot\nabla\phi_{i,j}. \tag{7}$$

Since P is a solution, the choice of each $c_{i,j}$ must be optimal. Then for any $0 \le i_0, j_0 \le n-1$, we have

$$\begin{aligned}
0 &= \frac{\partial D}{\partial c_{i_0,j_0}} = \frac{\partial\langle \boldsymbol{A_\theta} - \nabla P, \boldsymbol{A_\theta} - \nabla P\rangle}{\partial c_{i_0,j_0}}\\
&= \frac{\partial\langle \boldsymbol{A_\theta}, \boldsymbol{A_\theta}\rangle}{\partial c_{i_0,j_0}} + \frac{\partial\langle \nabla P, \nabla P\rangle}{\partial c_{i_0,j_0}} - 2\frac{\partial\langle \boldsymbol{A_\theta}, \nabla P\rangle}{\partial c_{i_0,j_0}}\\
&= 0 + \sum_{0\le i,j,k,l\le n-1} \frac{\partial\langle\nabla\phi_{i,j},\nabla\phi_{k,l}\rangle c_{i,j}c_{k,l}}{\partial c_{i_0,j_0}}\\
&+ \sum_{0\le i,j\le n-1} \frac{\partial\langle \boldsymbol{A_\theta},\nabla\phi_{i,j}\rangle c_{i,j}}{\partial c_{i_0,j_0}}\\
&= 2\sum_{0\le i,j\le n-1}\langle\nabla\phi_{i,j},\nabla\phi_{i_0,j_0}\rangle c_{i,j} - 2\langle \boldsymbol{A_\theta},\nabla\phi_{i_0,j_0}\rangle.
\end{aligned}$$

Therefore we get n^2 linear equations (for all pairs of $0 \le i_0, j_0 \le n-1$):

$$\sum_{0\le i,j\le n-1}\langle\nabla\phi_{i,j},\nabla\phi_{i_0,j_0}\rangle c_{i,j} - \langle \boldsymbol{A_\theta},\nabla\phi_{i_0,j_0}\rangle = 0. \tag{8}$$

Now we analyze the linear system (8). The coefficient matrix is $n^2 \times n^2$ and sparse.

Lemma 3. Let $0 \le i, j, k, l \le n-1$ be integers

1) $\langle\nabla\phi_{i,j},\nabla\phi_{i,j}\rangle = \frac{8u^2}{3}$;
2) if (i, j) and (k, l) are distinct pairs such that both i, k and j, l differ by at most 1 modulo n, then $\langle\nabla\phi_{i,j},\nabla\phi_{k,l}\rangle = -\frac{u^2}{3}$;
3) for all other (i, j) and (k, l), $\langle\nabla\phi_{i,j},\nabla\phi_{k,l}\rangle = 0$.

Lemma 3 follows from direct computations based on (6).

Proposition 4. The square matrix

$$A = \{\langle\nabla\phi_{i,j},\nabla\phi_{k,l}\rangle\}_{0\le i,j,k,l\le n-1}$$

has rank $n^2 - 1$.

Proof. By Lemma 3, the sum of the column vectors in A is the zero vector. So the all-one vector $\mathbf{1}$ belongs to the null space of A. In addition, by the symmetry and sparsity of A, there is no other linear dependence among the column vectors in A, so the rank of A is the size of A minus the dimension of the null space of A, which is $n^2 - 1$. □

By Proposition 4, the solution space of (8) has dimension 1. While it is easy to verify that $\sum_{0\le i,j\le n-1}\phi_{i,j}(r_1, r_2) \equiv 1$ for all $(r_1, r_2) \in T^2$. Hence any scaling to a solution of $c_{i,j}$'s would result in another solution, and at the level of $P(r_1, r_2)$ it only differs a constant with the previous one. So (8) gives a unique solution of $P(r_1, r_2)$ up to a constant scaling.

The values of $\langle\nabla\phi_{i,j},\nabla\phi_{k,l}\rangle$ could be computed from (6), and the values of $\langle \boldsymbol{A_\theta},\nabla\phi_{i_0,j_0}\rangle$ can be approximately computed using the values of $\boldsymbol{A_\theta}$ at lattice points near $\left(\frac{2\pi i_0}{n}, \frac{2\pi j_0}{n}\right)$.

Note that we applied similar approach to determine the Optimal choice of reference position [2], corresponds to finding the potential function of the first two rows of the local form of the connection matrix $\boldsymbol{A}(\boldsymbol{r})$.

IV. Results

We applied our robot approach to study the body-leg coordination of centipede locomotion. Biological centipedes have two distinct locomotion patterns [8], [9]: the direct-wave (leg wave propagating from tail to head) and the retrograde-wave (leg wave propagating from head to tail). The leg wave can be characterized by leg phase lag L [10], defined as the phase offset between two consecutive legs on the same side, where $L > 0.5$ indicates retrograde wave (fore-leading) and $L < 0.5$ indicates direct wave (hind-leading). Note that $L = 0$. Retrograde-wave centipedes moving at high speeds perform a characteristic body undulation, which is not present in direct-wave centipedes.

In previous work [1], a robophysical centipede model was built and the contribution of lateral body undulation to different leg waves was experimentally evaluated [1]. Experiments verified that lateral body undulation has greater contribution to the retrograde-wave gaits than the direct-wave gaits.

To study the body-leg coordination, we describe the centipede leg movements by its phase [5], [15], [7], denoted as $r_1 \in S^1$; similarly, we describe the lateral body undulation by its phase, denoted as $r_2 \in S^1$.

In the original framework of [7], we chose the head frame as the body frame (such that the head of centipede robot is always oriented horizontally, see Fig. 4a) to numerically calculate the local form of the connection $\boldsymbol{A}(\boldsymbol{r})$. An example of the vector field (the third row of the local form of the connection, $A_\theta(r)$), is plotted in Fig. 4a. The corresponding forward height function is plotted in Fig. 4b. The blue curve in Fig. 4 indicates the optimal $\partial\chi$ that enclosed the most surface area in the height function.

Note that the vector field in Fig. 4a has large norms. In this way, the Lie bracket can have significant effect on the quantitative prediction of displacement. In Fig. 4c, we showed the quantitative prediction of speed (measured in body length travelled per gait cycle) as a function of lateral phase lag L. From Fig. 4c, we note that the contribution from the body undulation is greater in the direct-wave centipedes than the retrograde-wave centipedes, which is against the observed pattern.

Authorized licensed use limited to: Georgia Institute of Technology. Downloaded on June 17,2021 at 16:03:22 UTC from IEEE Xplore. Restrictions apply.

We now applied our approach to minimize the Lie bracket effect, and numerically calculated the potential function associated with the vector field in Fig. 4a. By subtracting the gradient of the potential function, we obtained a new vector field (vector fields in the optimal body frame) in Fig. 5a. The norm of the new vector field is significantly less than that of the original vector field. We then calculated the corresponding height function in the optimal body frame in Fig. 5b. We observe that the pattern of the height function in the optimal body frame is different from the height function in the original body frame. However, both height function yields similar body-leg coordination pattern $\partial\chi$.

Next we compare the prediction on speed in the optimal frame (Fig. 5). We observe that in the optimal frame, we have agreement with the experimental results: the contribution from lateral body undulation is greater in the retrograde-wave centipedes than the direct-wave centipede, agreeing with the experimental data and the biological observations.

V. Discussion

In practice, some postures in the shape space are not allowed in the robot implementation. For example, some of them have self-intersections, which might cause damage to the motors. So these postures form the forbidden region in T^2 as a union of holes, and we may introduce a new shape space Ω, which is T^2 minus the forbidden region. In this case, our method could be adapted as follows:

(i) We discretize the holes by assuming that for each square in the mesh, it is either entirely contained in a hole, or disjoint from the holes.

(ii) For each lattice point, if at least one quadrant around it is not in a hole, then we define a basis function at this lattice point for the non-hole quadrants around it, in the same manner as in (6).

(iii) We can still establish a linear system of $c_{i,j}$'s, and the dimension of the solution space depends on the number of holes in Ω.

Acknowledgments

We appreciate the fruitful suggestions from Yingjie Liu on the project. This project is supported by the National Science Foundation and the Simons Foundation through the Southeast Center for Mathematics and Biology.

References

[1] Yasemin Ozkan-Aydin, Baxi Chong, Enes Aydin, and Daniel I. Goldman. A systematic approach to creating terrain-capable hybrid soft/hard myriapod robots. In IEEE International Conference on Soft Robotics (Robosoft), 2020.

[2] Ross L. Hatton and Howie Choset. Geometric motion planning: the local connection, Stokes' theorem, and the importance of coordinate choice. The International Journal of Robotics Research, 30(8):988–1014, 2011.

[3] Ross L Hatton, Yang Ding, Howie Choset, and Daniel I Goldman. Geometric visualization of self-propulsion in a complex medium. Physical review letters, 110(7):078101, 2013.

[4] Ross L. Hatton and Howie Choset. Nonconservativity and noncommutativity in locomotion. The European Physical Journal Special Topics, 224(17-18):3141–3174, 2015.

[5] Baxi Chong, Yasemin Ozkan Aydin, Chaohui Gong, Guillaume Sartoretti, Yunjin Wu, Jennifer M Rieser, Haosen Xing, Jeffery W Rankin, Krijn Michel, Alfredo G Nicieza, et al. Coordination of back bending and leg movements for quadrupedal locomotion. In Robotics: Science and Systems, 2018.

[6] Elie A Shammas, Howie Choset, and Alfred A Rizzi. Geometric motion planning analysis for two classes of underactuated mechanical systems. The International Journal of Robotics Research, 26(10):1043–1073, 2007.

[7] Chaohui Gong, Zhongqiang Ren, Julian Whitman, Jaskaran Grover, Baxi Chong, and Howie Choset. Geometric motion planning for systems with toroidal and cylindrical shape spaces. In ASME 2018 Dynamic Systems and Control Conference. American Society of Mechanical Engineers Digital Collection, 2018.

[8] B Anderson, J Shultz, and B Jayne. Axial kinematics and muscle activity during terrestrial locomotion of the centipede scolopendra heros. Journal of Experimental Biology, 198(5):1185–1195, 1995.

[9] Shigeru Kuroda, Itsuki Kunita, Yoshimi Tanaka, Akio Ishiguro, Ryo Kobayashi, and Toshiyuki Nakagaki. Common mechanics of mode switching in locomotion of limbless and legged animals. Journal of the Royal Society interface, 11(95):20140205, 2014.

[10] SM Manton. The evolution of arthropodan locomotory mechanisms—part 3. the locomotion of the chilopoda and pauropoda. Zoological Journal of the Linnean Society, 42(284):118–167, 1952.

[11] Jerrold E Marsden and Tudor S Ratiu. Introduction to mechanics and symmetry: a basic exposition of classical mechanical systems, volume 17. Springer Science & Business Media, 2013.

[12] SV Walker and RI Leine. Set-valued anisotropic dry friction laws: formulation, experimental verification and instability phenomenon. Nonlinear Dynamics, 96(2):885–920, 2019.

[13] Masashi Saito, Masakazu Fukaya, Tetsuya Iwasaki, et al. Modeling, analysis, and synthesis of serpentine locomotion with a multilink robotic snake. IEEE control systems magazine, 22(1):64–81, 2002.

[14] R.E. Williamson and H.F. Trotter. Multivariable Mathematics. Pearson Prentice Hall, 2004.

[15] Baxi Chong, Yasemin Ozkan Aydin, Guillaume Sartoretti, Jennifer M Rieser, Chaohui Gong, Haosen Xing, Howie Choset, and Daniel I. Goldman. A hierarchical geometric framework to design locomotive gaits for highly articulated robots. In Robotics: science and systems, 2019.

Authorized licensed use limited to: Georgia Institute of Technology. Downloaded on June 17,2021 at 16:03:22 UTC from IEEE Xplore. Restrictions apply.